Effectively combining NMR measurements and capillary pressure saturation data: A new joint inversion approach

Thomas Hiller and Norbert Klitzsch
Institute for Applied Geophysics and Geothermal Energy, RWTH Aachen, Mathieustr. 10, 52074 Aachen, Germany

This paper was prepared for presentation at the International Symposium of the Society of Core Analysts held in Vienna, Austria, 27 August – 1 September 2017

ABSTRACT

Nuclear magnetic resonance (NMR) relaxation measurements are a well established laboratory and bore-hole method to characterize the storage and transport properties of rocks due to its direct sensitivity to the corresponding pore fluid content (water / oil) and pore sizes. Thereby, the correct estimation of these properties depends strongly on the underlying pore model. Commonly, cylindrical capillaries or spherical pores are assumed for interpreting NMR relaxation data. However, for deducing the size of these pores and thus the pore size distribution (PSD) from the NMR relaxation time distribution a calibration of the NMR data is necessary. Here, we present a novel joint inversion approach of NMR relaxation and capillary pressure saturation (CPS) data based on an angular pore model. This inversion (1) omits the need for the aforementioned calibration and can therewith be used to directly determine the PSD of the sample; (2) accounts for residual water by taking advantage of the angular pore model and (3) can determine the shape of the angular pores by using NMR data measured at both the drainage and the imbibition branch. We show the applicability of the joint inversion approach with angular pores on different synthetic and experimental data sets.

INTRODUCTION

Multi-phase fluid flow through porous media plays an important role in many geoscientific and geotechnical applications and is therefore subject to a broad range of research projects. Especially in the context of reservoir characterization (be it water or hydrocarbon reservoirs), the determination of petrophysical parameters like e.g. porosity and permeability is of utmost importance. These parameters are then further used to characterize the transport and storage properties of rocks or soils e.g. the ability to conduct fluids through its pore space and are the basis of a profound reservoir evaluation.

Among other methods, NMR has been proven to be a viable tool in order to directly or indirectly determine these petrophysical parameters. With its direct sensitivity to hydrogen protons, NMR can be used to noninvasively determine water content. Furthermore, the NMR relaxation behavior is directly related to the surface-to-volume ratio of the pore space and can therefore be used to determine the corresponding PSD. However, the link between NMR relaxation times and pore sizes, generally involves a calibration procedure via the surface relaxivity ρ_s which itself is a sample dependent parameter [1, 2].

If the pore space contains water and air, only the water contributes to the NMR signal. Several attempts have been made to derive transport properties directly from NMR measurements [3-5]. This works sufficiently well, e.g., for sediments and conventional reservoirs but has limitations when a considerable amount of clay minerals is present or the pore space is very heterogeneous, like e.g. in carbonate rocks [6]. Additionally, also a non-uniform distribution of surface relaxivities within a rock may strongly influence the NMR signal and simple NMR-permeability relationships break down (e.g. [7]).

One way to account for a heterogeneous pore space is to consider angular pores. They can be used to explain the typical shift in relaxation time distributions to smaller relaxation times when draining an initially fully saturated sample [8]. In this work we employ angular pores to the joint inversion approach proposed by [9]. This joint inversion combines NMR and CPS data at different levels of saturation to directly invert for the PSD and surface relaxivity ρ_{s}. Furthermore, we present a method that allows to additionally invert for the cross-sectional shape of our angular pore model by using NMR data from the CPS hysteresis (drainage and imbibition) simultaneously. We like to point out that our employed pore model of a capillary bundle is still a strong simplification of the real pore space. Especially when considering the advancement that has been made in recent years to study two-phase fluid flow processes on the pore scale. However, the presented method allows for a fast and reliable estimation of macroscopic transport processes on the sample scale.

BASICS OF NMR RELAXATION

The NMR relaxation mechanism results from the interaction of a porous medium with its pore-filling fluid (usually water) containing a detectable amount of Hydrogen protons H^+. In most laboratory and well-logging applications, the Hydrogen protons are aligned with a strong static magnetic field $\mathbf{B}$. The characteristic precession frequency of protons around this static magnetic field is called Larmor frequency $\omega_L = \gamma_H \mathbf{B}_0$ and solely depends on the strength of $\mathbf{B}_0$ and the gyromagnetic ratio γ_H of Hydrogen. A NMR relaxation measurement is started by applying an energizing electromagnetic pulse with the corresponding devices' Larmor frequency and thus tipping away all Hydrogen protons from their equilibrium state. After the pulse is switched off, the protons can relax back into their equilibrium state. The relaxation process is described by the macroscopic phenomenological Bloch equations with their corresponding solutions

$$\begin{aligned} M_{\mathrm{z}}(t) &= \mathbf{M}_0 \left[1 - e^{-\frac{t}{T_1}}\right] \\ M_{\mathrm{xy}}(t) &= \mathbf{M}_0 e^{\frac{-t}{T_2}} \end{aligned} \tag{1}$$

where $\mathbf{M}_0$ is the equilibrium magnetization and M_{z} and M_{xy} are the longitudinal and transversal magnetization, respectively. Here, we only focus on the transversal magnetization and its corresponding relaxation constant T_2. The NMR relaxation process is a superposition of three independent mechanisms [4, 5]. The bulk relaxation T_{b} of the pore fluid, the surface relaxation T_{s} due to the interaction of pore fluid and rock matrix and diffusional relaxation T_{d} (only for transversal relaxation) caused by magnetic field gradients. If we assume the fast diffusion regime, which is reasonable for natural porous

media under consideration, the surface relaxation dominates and diffusional relaxation can safely be neglected. Then, the transversal relaxation time T_2 is given by

$$\frac{1}{T_2} = \frac{1}{T_{2,\mathrm{b}}} + \frac{1}{T_{2,\mathrm{s}}} = \frac{1}{T_{2,\mathrm{b}}} + \rho_{\mathrm{s}} \frac{S}{V}, \tag{2}$$

where ρ_{s} is the surface relaxivity and S/V the surface-to-volume ratio of the porous medium. Generally, one can deduce the following straightforward relationship from equation 2: the larger the pore the longer is the relaxation time T_2 and vice versa. To calculate a multi-exponential NMR relaxation signal, equations 1 and 2 can readily be combined

$$\frac{M_{\mathrm{xy}}(t)}{\mathbf{M}_0} = \sum_i \frac{V_i}{V_0} e^{\frac{-t}{T_{2,i}}} = \sum_i \frac{V_i}{V_0} e^{-t\left(\frac{1}{T_{2,\mathrm{b}}} + \rho_{\mathrm{s}} \frac{S_i}{V_i}\right)}, \tag{3}$$

with V_0 being the total water-filled pore volume. S_i and V_i denote the individual surface area and volume of pore class i relaxing with the characteristic relaxation time $T_{2,i}$. From equation 3 one can see that at full saturation the magnetization $\mathbf{M}_0$ is proportional to the total pore volume V_0 and hence relates signal strength to water content of the saturated sample. This enables NMR to be a direct method to determine the water content of a given sample and to deduce from this i.e. also the porosity.

JOINT INVERSION WITH ANGULAR PORES

[9] has introduced a joint inversion approach that allows to combine several NMR measurements at different levels of saturation, e.g. during a drainage process. By using the Young-Laplace relation

$$p \propto \frac{1}{R} \tag{4}$$

as a constraint, where p is pressure and R the radius of a cylindrical pore, and equation 3, he could directly infer from the joint inversion the surface relaxivity ρ_{s} and hence, the PSD.

We extend this approach so that pores with a triangular cross-section can also be considered. In the case of full saturation, the NMR signal of a single angular pore depends only on its volume (amplitude) and total surface-to-volume ratio (relaxation time). In contrast to cylindrical pores, angular pores are not completely desaturated but water remains in the pore corners. Thus, the partially saturated pores contribute to the NMR signal too. The radius R in equation 4 corresponds to the radius of the arc menisci R_{AM} in the corner of a partially filled angular pore (cf. Figure 1). From geometrical relations based on the works of [10, 11] it is possible to deduce the partial saturation of an angular pore based on the applied pressure. Similar to equation 3 one can calculate a NMR relaxation signal for a single angular pore after [8]

$$\frac{M_{\mathrm{xy}}(t)}{\mathbf{M}_0} = \sum_c \frac{V_c}{V_{\Delta 0}} e^{-t\left(\frac{1}{T_{2,\mathrm{b}}} + \rho_{\mathrm{s}} \frac{S_c}{V_c}\right)}, \tag{5}$$

where c is the corner index, $V_{\Delta 0}$ the volume of the single angular pore and S_c and V_c the surface and volume of the corresponding corner, respectively. The above relations for angular pores can be combined with the joint inversion approach from [9]

$$\mathbf{d} = \mathbf{G}\mathbf{m}\,, \tag{6}$$

where $\mathbf{d} = \left[M_{\mathrm{xy}}(t)/\mathbf{M}_0\right]_n$ is the data vector holding all n NMR signals, $\mathbf{m} = V_i/V_0$ is the model vector representing the PSD and $\mathbf{G}$ is the forward operator that describes the relationship between model and data (equation 5). For different pressure steps p_n the entries of

$$\mathbf{G}_i(\rho_{\mathrm{s}}, p_n) = \begin{cases} \sum_i e^{-t\left(\frac{1}{T_{2,\mathrm{b}}}+\rho_{\mathrm{s}}\frac{S_i}{V_i}\right)} & p_n < p_{\mathrm{crit},i} \\ \sum_i \sum_c \frac{V_{c,i}}{V_{\Delta 0}} e^{-t\left(\frac{1}{T_{2,\mathrm{b}}}+\rho_{\mathrm{s}}\frac{S_{c,i}}{V_{c,i}}\right)} & p_n \geq p_{\mathrm{crit},i} \end{cases}, \tag{7}$$

depend on the critical pressure p_{crit} of the corresponding pore size class i. If the pressure is smaller than the critical pressure $p_n < p_{\mathrm{crit},i}$ the pore class i is fully saturated. If, on the contrary, the pressure is larger than the critical pressure $p_n \geq p_{\mathrm{crit},i}$ pore class i is partially saturated and the contributions of the three corners c need to be considered. Note that, in the case of cylindrical pores $\mathbf{G}_i\left(\rho_s, p_n \geq p_{\mathrm{crit},i}\right) = 0$, the entries of the forward operator are zero due to the full-empty characteristic [9]. The non-linear system of equations in equation 6 can now be solved for $\mathbf{m}$ and ρ_{s} simultaneously by applying, e.g., a regularized (damped) Levenberg-Marquardt algorithm [9,12, 13]. To all inversions presented in this work a first-order smoothness constraint was employed [14] and the inversion is regularized so that the final NMR data misfit is of the same order as the data noise.

First, we use a synthetic model with a cross-sectional shape of $[90°, 60°, 30°]$ and surface relaxivity $\rho_{\mathrm{s}} = 10\ \mu\mathrm{ms}^{-1}$ to demonstrate the joint inversion with angular pores (Figure 2). T_2 NMR signals are calculated at four different levels of saturation and superposed by 0.5% Gaussian noise to simulate a signal-to-noise ratio (SNR) of 200, which is a reasonable value for laboratory NMR measurements (Figure 2c). In each sub-panel of Figure 2 the red lines indicate the corresponding fits or inverted model, respectively. Combining these four signals and applying an angular inversion model yields an almost perfect fit to the forward model (Figure 2a) with an inverted surface relaxivity of $\rho_{\mathrm{s}} = 10.02\ \mu\mathrm{ms}^{-1}$. The CPS-curve fit also agrees nicely with the forward model (Figure 2b).

APPLICATION TO REAL DATA

Now we apply our joint inversion approach to two different laboratory samples (Figure 3). The first one is a sintered borosilicate, generally used as filter material, with a very homogeneous grain and pore structure and a porosity of $\Phi \approx 0.3$ (Figure 3a). The measured intrinsic gas permeability is $k_{\mathrm{int(gas)}} = 7\mathrm{d}$. The second one is a coarse-grained sandstone from a tight gas reservoir with a porosity of $\Phi \approx 0.1$ (Figure 3b). The measured

intrinsic gas permeability is $k_{\mathrm{int(gas)}} = 10\mu\mathrm{d}$, which is more than four orders of magnitude smaller compared to the borosilicate sample.

Example 1 – Sintered Borosilicate
Figure 4 shows the joint inversion applied to NMR data acquired on a sintered borosilicate sample during a drainage experiment. [9] already used this data set to initially present the joint inversion with cylindrical pores. One particular drawback of a cylindrical pore model, when applied to real data, is its inability to account for residual water in pore crevices, which was also reported by [9]. We use seven NMR signals (Figure 4c) measured at decreasing saturations from 100% (black) to 7% (yellow). In contrast to the cylindrical pore model presented in [9], the joint inversion with angular pores gives a unimodal PSD (Figure 4a) with a peak at $x \approx 2\mathrm{x}10^{-5}\mathrm{m}$ and therewith fits much better to the Mercury Injection Capillary Pressure (MICP) data. Note, that MICP data generally yields pore throat sizes and not pore sizes due to the non-wetting character of mercury. Considering the very narrow MICP distribution and the slight shift of the NMR PSD mode to larger values compared to the MICP data, the two data sets agree very well with each other. Finally, also the fitted CPS-curve matches the experimental data nicely (Figure 3b).

Example 2 – Tight Gas Sandstone
Figure 5 shows the inversion result for the tight gas reservoir sandstone. The sample was installed in a high-pressure flow cell with a confining pressure of $p_{\mathrm{conf}} = 15$ MPa and continuously drained with nitrogen gas and increasing differential pressures up to $\Delta p = 2.5$ MPa [15]. The inherent differences between these two samples is strongly reflected in the measured NMR signals. Note that the time axis of Figure 5c is in log-scale to better distinguish between the individual signals especially at partial saturation. Also the applied drainage pressures are an order of magnitude larger compared to the borosilicate sample. The inverted PSD shows a slight trimodal character with the major peak (mode) at $x \approx 3\mathrm{x}10^{-7}\mathrm{m}$.

As a cross check, we estimate the permeability of the inverted PSD for both samples by a simple Kozeny-Carman-type [16] relation

$$k_{\mathrm{NMR}} = \frac{\Phi R_{\mathrm{lgm}}^2}{8\tau}, \tag{8}$$

with porosity Φ and R_{lgm} equal to the logarithmic mean radius of the PSD. We assume tortuosity $\tau = 1$ because we have no information about it. Thus, we may overestimate the permeability. We obtain $k_{\mathrm{NMR}} = 5.9\mathrm{d}$ and $k_{\mathrm{NMR}} = 33\mu\mathrm{d}$ as permeabilities for the borosilicate and sandstone sample, respectively. Even though our permeability estimation may be strongly simplified and considering the quite simple pore model of a capillary bundle, the derived values are exceptionally close to the measured data.

USING THE JOINT INVERSION TO DETERMINE PORE SHAPE

Additional to PSD and surface relaxivity, the shape of the angular pore can be determined by the introduced inversion approach, if NMR data during drainage and imbibition are considered. This is due to the drainage and imbibition hysteresis of angular pores, which

solely depends on their shape [8, 11]. Figure 6 demonstrates this exemplary for a synthetic model with a cross-sectional shape of $[90°, 80°, 10°]$ and a surface relaxivity of $\rho_s = 10\ \mu ms^{-1}$. Figure 6a-c shows the joint inversion result if only drainage data is used. Although the inverted surface relaxivity $\rho_s = 10.6\ \mu ms^{-1}$ is close to the given value, the inverted angular shape is far off $[90°, 59.5°, 30.5°]$. Due to the deviation in the inverted shape (Figure 6a) also the fitted imbibition branch of the CPS-curves does not fit with the forward model (Figure 6b). In Figure 6d-f the NMR signal at 50% saturation is taken from the imbibition branch. Now, not only the surface relaxivity $\rho_s = 9.9\ \mu ms^{-1}$ fits well to the forward model but also the inverted angular shape $[90°, 79.9°, 10.1°]$ and, hence, the CPS-curves.

We tested this approach for triangular shapes ranging from $[90°, 89°, 1°]$ to $[90°, 45°, 45°]$ and found exceptionally well fits, especially for very acute triangular shapes up to $[90°, 65°, 25°]$. For less acute triangular shapes the difference in the inverted shape is generally off by $\approx 5°$. This however, is to be expected due to the decreasing hysteresis for less acute triangles [17].

SUMMARY

We presented a joint inversion approach for NMR data at different water saturations using an angular pore-bundle model. This joint inversion provides the PSD and surface relaxivity of the studied samples. The implementation of angular pores allows the consideration of residual water in pore crevices and hence considerably improves the robustness of the method. Additionally, it is also possible to estimate the permeability of the measured samples even though the applied pore model (capillary bundle) is a strong simplification of a real porous medium. We have also shown that we can additionally invert for the shape of the angular pores when both, the drainage and imbibition branches of a CPS hysteresis are used. So far the latter was shown for synthetic data only because of lacking NMR data at the imbibition path.

ACKNOWLEDGEMENTS

The authors gratefully acknowledge Wintershall Holding GmbH for funding the iLoPS project within this study was prepared.

REFERENCES

1. Torrey, H.C., “Bloch Equation with Diffusion Terms”, *Physical Review*, (1956) **104**, 563-565
2. Brownstein, K.R. and Tarr, C.E., “Importance of classical diffusion in NMR studies of water in biological cells”, *Physical Review A*, (1979) **19**, 2446
3. Kenyon, W.E., “Petrophysical Principles of Applications of NMR Logging”, *The Log Analyst*, (1997) **38**, 21-43
4. Coates, G.R., Xiao, L. and Prammer, M.G., *NMR logging: principles and applications*, Gulf Professional Publishing, 1999
5. Dunn, K.-J., Bergman, D.J. and LaTorraca, G.A., *Nuclear magnetic resonance: petrophysical and logging applications*, Handbook of Geophysical Exploration Vol. 32, Elsevier, 2002

6. Westphal, H., Surholt, I., Kiesl, C., Thern, H.F. and Kruspe, T. „NMR Measurements in Carbonate Rocks: Problems and an Approach to a Solution", *pure and applied geophysics*, (2005),**162**, 549-570
7. Costabel, S. and Yaramanci, U., "Estimation of water retention parameters from nuclear magnetic resonance relaxation time distributions", *Water Resources Research*, (2013), **49**, 2068-2079
8. Mohnke, O., Jorand, R., Nordlund, C. and Klitzsch, N., „Understanding NMR relaxometry of partially water saturated rocks", *Hydrology and Earth System Sciences*, (2015), **19**, 2763-2773
9. Mohnke, O., "Jointly deriving NMR surface relaxivity and pore size distributions by NMR relaxation experiments on partially desaturated rocks", *Water Resources Research*, (2014), *50*, 5309-5321
10. Mason, G. and Morrow, N.R., "Capillary behavior of a perfectly wetting liquid in irregular triangular tubes", *Journal of Colloid and Interface Science*, (1991), **141**, 262-274
11. Tuller, M, Or, D. and Dudley, L.M., "Adsorption and capillary condensation in porous media: Liquid retention and interfacial configurations in angular pores", *Water Resources Research*, (1999), **35**, 1949-1964
12. Levenberg, K., "A method for the solution of certain problems in least-squares", *Quarterly of Applied Mathematics*, (1944), **2**, 164-168
13. Marquardt, D.W., "An Algorithm for Least-Squares Estimation of Nonlinear Parameters", *Journal* of the *Society* for *Industrial* and *Applied Mathematics*, (1963), **11**, 431-441
14. Aster, R.C., Borchers, B. And Thurber, C.H., *Parameter Estimation and Inverse Problems*, Academic Press, 2013
15. Hoder, G., *Monitoring of Two-Phase Fluid Flow Experiments by NMR*, MSc thesis, RWTH Aachen University, 2016
16. Carman, P.C., *Flow of gases through porous media*, Academic Press, New York, 1956
17. Hiller, T. and Klitzsch, N. *Joint Inversion of NMR and desaturation data using an angular pore model*, 76. General Assembly of the German Geophysical Society, 2016

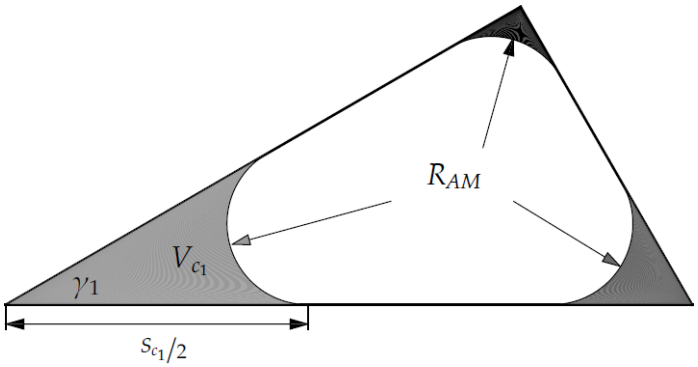

Figure 1. Cross-section of a triangular pore (water-gray, air-white). The pressure dependent radius of the arc menisci is the same in every corner of a triangle irrespective of the individual corner angle γ. S_c and V_c are the surface and volume of the corresponding corner and determine the individual relaxation time T_2 after equation 5.

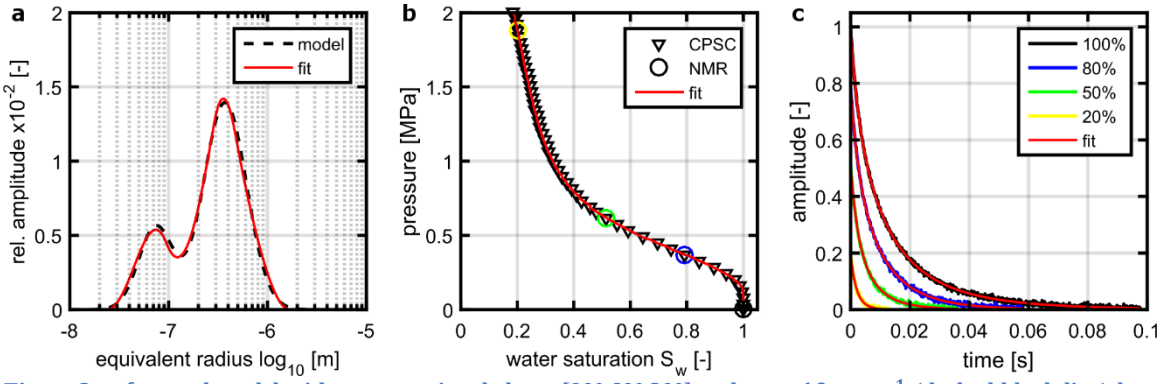

Figure 2 a: forward model with cross-sectional shape [90°,60°,30°] and $\rho_s = 10$ µms^{-1} (dashed black line) b: corresponding CPS curve (black downward triangles), color-coded are the saturation levels where a NMR signal was calculated (circles) c: NMR signals (with 0.5% Gaussian noise) at the corresponding saturation levels (from black – full saturation to yellow – 20% saturation); in all three sub-panels the red lines show the inversion results, the inverted surface relaxivity is $\rho_s = 10.02$ µms^{-1}.

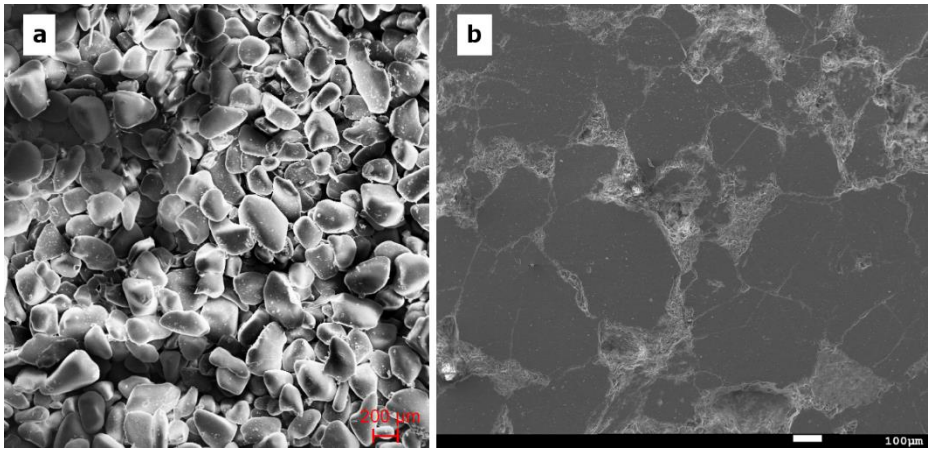

Figure 3 SEM images of the two samples used in this study a: sintered borosilicate with a quite homogeneous grain size structure. The red scale refers to 200µm b: tight sandstone with coarse-grained structure and irregular angular pores.

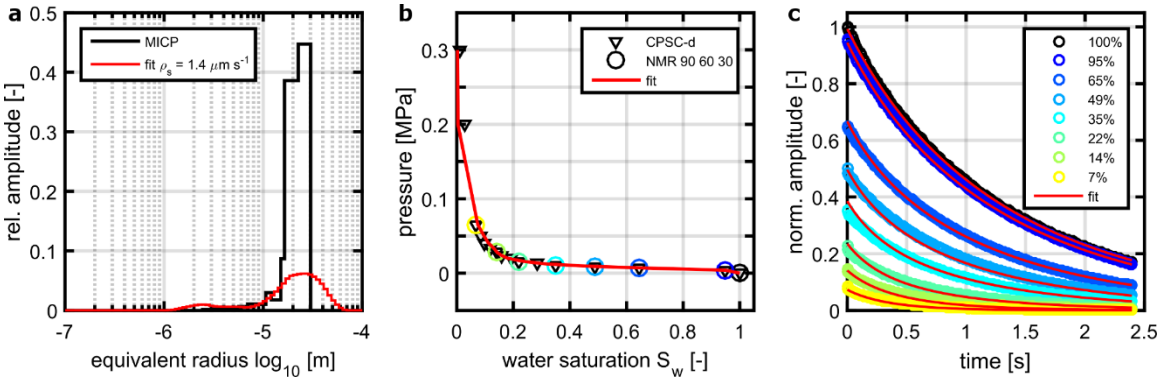

Figure 4 Joint inversion results of the NMR data set for a sintered borosilicate sample measured at decreasing levels of saturation and using an angular pore [90°,45°,45°] a: Mercury Injection Capillary Pressure (MICP) curve (black) b: corresponding CPS curve (black downward triangles); color-coded are the saturation levels where a NMR signal was measured (circles); Note that the full saturation signal (O – 100%) was measured at 0 Pa and is plotted here at 1x10³ Pa for visualization purposes only. c: NMR signals at the corresponding saturation levels (from black – full saturation to yellow – 7% saturation); in all three sub-panels the red lines show the inversion results, the inverted surface relaxivity is $\rho_s = 1.4$ µms^{-1}.

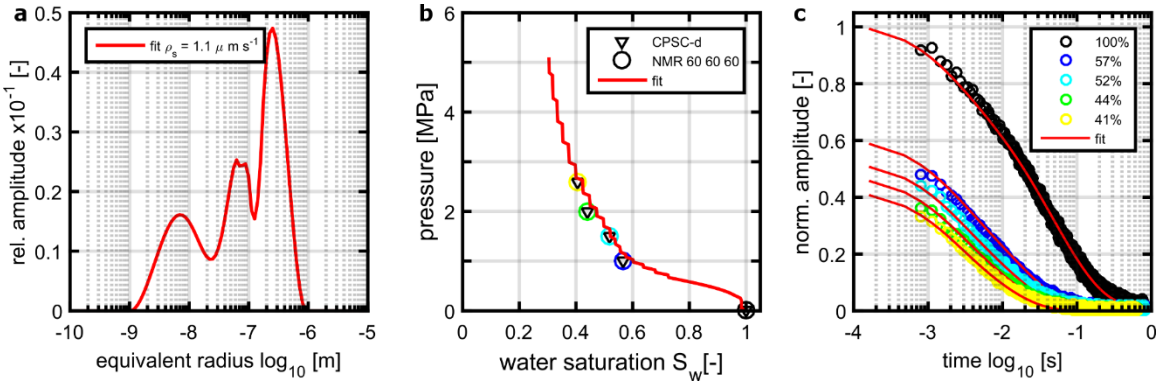

Figure 5 Joint inversion results of the NMR data set for a tight sandstone sample measured at decreasing levels of saturation and using an angular pore model [60°,60°,60°] a: inverted PSD (red) b: corresponding CPS curve (black downward triangles), color-coded are the saturation levels where a NMR signal was measured (circles) c: NMR signals at the corresponding saturation levels (from black – full saturation to yellow – 41% saturation); in all three sub-panels the red lines show the inversion results, the inverted surface relaxivity is $\rho_s = 1.1\ \mu\text{ms}^{-1}$.

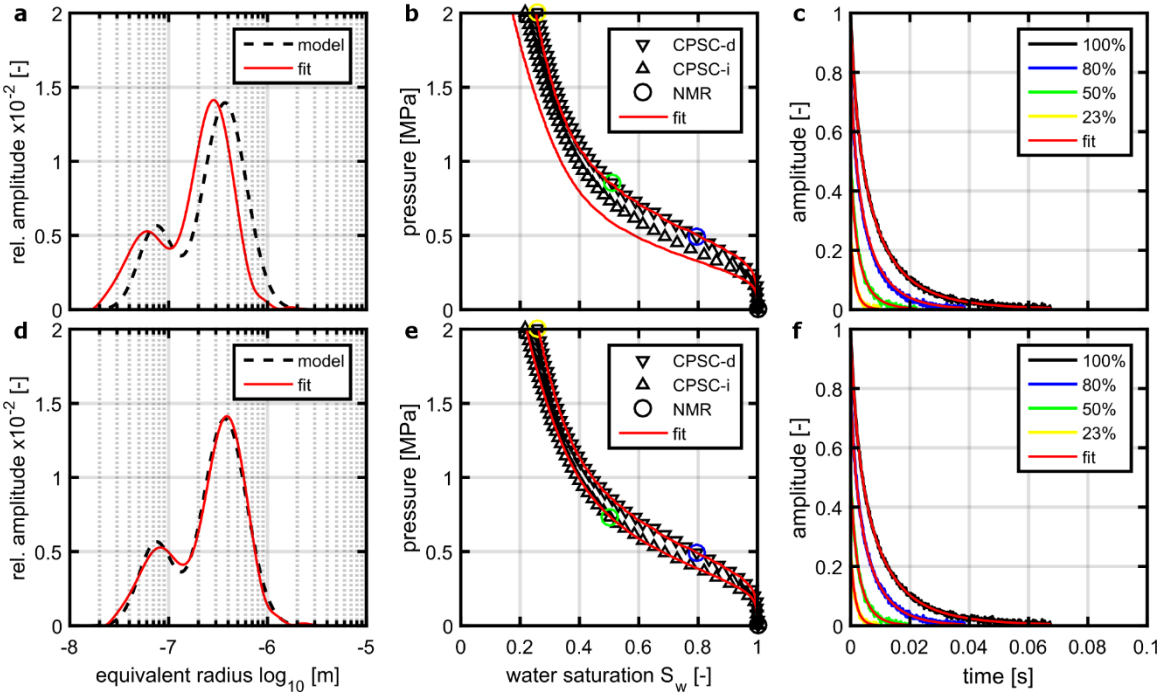

Figure 6 Joint inversion for surface relaxivity ρ_s and pore shape angle α when using synthetic NMR signals either only during drainage (a-c) or during drainage and imbibition (d-f); a+d: forward model with cross-sectional shape [90°,80°,10°] and surface relaxivity $\rho_s = 10\ \mu\text{ms}^{-1}$ (dashed black line) b+e: corresponding CPS curve (black downward triangles – drainage, black upward triangles - imbibition), color-coded are the saturation levels where a NMR signal was calculated (circles) c+f: NMR signals (with 0.5% Gaussian noise) at the corresponding saturation levels (from black – full saturation to yellow – 23 % saturation); in all six sub-panels show the inversion results; when using drainage only the inverted angle and surface relaxivity are $\alpha_{\text{inv}} = 30.5°$ and $\rho_s = 10.6\ \mu\text{ms}^{-1}$ (a-c); when using drainage and imbibitions the inverted angle and surface relaxivity are $\alpha_{\text{inv}} = 10.1°$ and $\rho_s = 9.9\ \mu\text{ms}^{-1}$ (d-f).